AIP | Journal of Applied Physics

Crystal structure, electrical properties, and mechanical response of (100)-/(001)-oriented epitaxial Pb(Mg1/3Nb2/3)O3–PbTiO3 films grown on (100)cSrRuO3(100)SrTiO3 substrates by metal-organic chemical vapor deposition

Shintaro Yokoyama, Satoshi Okamoto, Hiroshi Funakubo, Takashi Iijima, Keisuke Saito et al.

Citation: J. Appl. Phys. **100**, 054110 (2006); doi: 10.1063/1.2337391
View online: http://dx.doi.org/10.1063/1.2337391
View Table of Contents: http://jap.aip.org/resource/1/JAPIAU/v100/i5
Published by the American Institute of Physics.

Crystal structure, electrical properties, and mechanical response of (100)-/(001)-oriented epitaxial $Pb(Mg_{1/3}Nb_{2/3})O_3-PbTiO_3$ films grown on $(100)_cSrRuO_3\|(100)SrTiO_3$ substrates by metal-organic chemical vapor deposition

Shintaro Yokoyama,[a] Satoshi Okamoto, and Hiroshi Funakubo[b]
Department of Innovative and Engineered Materials, Interdisciplinary Graduate School of Science and Engineering, Tokyo Institute of Technology, J2-43, 4259 Nagatsuta-cho, Midori-ku, Yokohama 226-8502, Japan

Takashi Iijima
Research Institute of Instrumentation Frontier, National Institute of Advanced Industrial Science and Technology, 1-1-1 Umezono, Tsukuba 305-8568, Japan

Keisuke Saito
Application Laboratory, Bruker AXS, 3-9-A, Moriya-cho, Kanagawa-ku, Yokohama 221-0022, Japan

Hirotake Okino and Takashi Yamamoto
Department of Communications Engineering, National Defense Academy, 1-10-20 Hashirimizu, Yokosuka, Kanagawa 239-8686, Japan

Ken Nishida and Takashi Katoda
Department of Electronic and Photonic Systems Engineering, Kochi University of Technology, 185 Miyanokuchi, Tosayamada, Kami-gun, Kochi 782-8502, Japan

Joe Sakai
School of Materials Science, Japan Advanced Institute of Science and Technology (JAIST), 1-1 Asahidai, Nomi, Ishikawa 923-1292, Japan

(Received 22 November 2005; accepted 24 June 2006; published online 12 September 2006)

Relaxor-type ferroelectric $(1-x)Pb(Mg_{1/3}Nb_{2/3})O_3-xPbTiO_3$ (PMN-PT) films, 2–3 μm in thickness, with a $PbTiO_3$ content (x) ranging from 0 to 1 were grown on $(100)_cSrRuO_3\|(100)SrTiO_3$ substrates at 650 °C by metal-organic chemical vapor deposition. The effects the x value had on the crystal structure, dielectric and ferroelectric properties, and mechanical response of these films were systematically investigated. Epitaxial growth having (100)/(001) orientation irrespective of x and the constituent phase change with x were ascertained from both x-ray diffraction reciprocal space mapping analysis and Raman spectroscopy. The constituent phase changed from a rhombohedral (pseudocubic) single phase, a mixture phase of rhombohedral (pseudocubic) and tetragonal phases, and a tetragonal single phase, with increasing x. The mixed phase region was found to exist at $x=0.40-0.55$, which was different from that reported for single crystals ($x=0.31-0.35$). The dependencies of relative dielectric constant and remanent polarization on x showed a similar trend in the case of a PMN-PT sintered body; however, the magnitudes of these values were relatively low. The effective longitudinal piezoelectric coefficient ($d_{33,f}$) and the transverse coefficient ($e_{31,f}$) of 100–120 pm/V and ~ -11.0 C/m^2 were, respectively, calculated for a film with $x=0.39$, which corresponds to a larger x edge for the rhombohedral (pseudocubic) region following the engineered domain concept proposed for PMN-PT single crystals. © *2006 American Institute of Physics*. [DOI: 10.1063/1.2337391]

I. INTRODUCTION

Lead magnesium niobate [$Pb(Mg_{1/3}Nb_{2/3})O_3$ (PMN)] with a perovskite structure is a classical relaxor ferroelectric material exhibiting diffuse phase transition and frequency-dependent dielectric maximum temperature.[1] Giant piezoelectric responses have been observed in single crystal solid solutions of PMN and $PbTiO_3$ [$(1-x)$PMN–xPT (PMN-PT)]. Shrout *et al.*[2] and Park and Shrout,[3] for example, reported a longitudinal piezoelectric coefficient (d_{33}) as high as 1500 pC/N along the [001] direction for the rhombohedral side of the near morphotropic phase boundary (MPB), at $x=0.30-0.35$, where the symmetry changes from rhombohedral (pseudocubic) to tetragonal for single crystals in the PMN-PT system. They suggested an engineered domain structure, where there is no driving force for non-180° domain wall motion in the case of a well-poled (001)-oriented rhombohedral crystal measured in the normal direction. The concept of whether an engineered domain exists is interesting from the standpoint of piezoelectric films since ferroelastic wall motion is difficult to achieve in many ferroelectric thin films.[4]

[a]Electronic mail: yokoyama@iem.titech.ac.jp
[b]Electronic mail: funakubo@iem.titech.ac.jp

We need to generate large strains for applications in microelectromechanical systems (MEMSs), which are the most attractive in the piezoelectric field, or sense very small ones, in thin constrained piezoelectric layers. This is because a large piezoelectric response (higher piezoelectric coefficient) offers the possibility of more sensitive sensors and lower voltage actuators. There is a significant potential for integrating this material into such piezoelectric applications and electronic devices if high-quality films can be fabricated. However, the systematic preparation of PMN-PT films for a wide x range is limited, particularly those with in- and out-of-plane piezoelectric responses, although these piezoelectric responses are very sensitive to film composition and it is very important to optimize them. The primary reason for the lack of literature on compositional effects has been the difficulty in obtaining a perovskite single phase for PMN-PT for a wide x range due to the relatively poor thermodynamic stability of the perovskite relative to the pyrochlore phase[5] and due to the compositional complexity of the solid solution. In addition, we need to grow highly oriented or epitaxial PMN-PT films so that we can explore their anisotropic piezoelectric and ferroelectric properties.

Of the various techniques used for preparing PMN-PT film, such as sol-gel,[6] sputtering,[7] and pulsed laser deposition,[8] metal-organic chemical vapor deposition[9,10] (MOCVD) has significant advantages in controlling composition,[11] film thickness uniformity, high deposition rate, and scalability in large deposition areas.

We demonstrated the systematic growth of (100)-/(001)-oriented epitaxial PMN-PT films for a wide x range from 0 to 1 by MOCVD and investigated the wide x range compositional dependencies of the crystal structure and electrical properties of these films.[12] Both in- and out-of-plane piezoelectric responses were found to be maximum at the higher x edge in the rhombohedral (pseudocubic) phase region, despite the fact that a mixed phase region of the rhombohedral (pseudocubic) and tetragonal phases lied on a different composition to that of single crystals. In the present study, the crystal structure, dielectric and ferroelectric properties, and mechanical response are discussed from the perspective of residual strain.

II. EXPERIMENT

$(1-x)$PMN$-x$PT films, 2–3 μm in thickness, were grown on $(100)_c SrRuO_3 \| (100)SrTiO_3$ substrates at 650 °C by pulsed MOCVD.[13] Conductive epitaxial $SrRuO_3$ films were used as the bottom electrode and were epitaxially grown on $(100)SrTiO_3$ substrates at 750 °C by MOCVD using $Sr(C_{11}H_{19}O_2)_2(C_8H_{23}N_5)_2$, $Ru(C_7H_{11})(C_7H_9)$ (Tosoh Corp.), and oxygen as sources.[14] The pseudocubic Miller index of crystal, designated in brackets as $(hkl)_c$, was used for $SrRuO_3$. The resulting substrates were $(100)_c SrRuO_3 \| (100)SrTiO_3$. $Pb(C_{11}H_{19}O_2)_2$, $Ti(O \cdot i\text{-}C_3H_7)_4$, $Mg(C_{14}H_{25}O_2)_2$ (Asahi Denka Corp.), and $Nb(O \cdot C_2H_5)_5$ were used as Pb, Ti, Mg, and Nb source materials, respectively. Oxygen was used as the oxidant gas and nitrogen as the carrier gas. The source gas mixture flowed to the substrates through a nozzle in a cold-wall-type vertical reaction chamber. The Ti/(Mg+Nb+Ti) ratio corresponding to x in the films was varied by controlling the concentration of the input source gases under a constant Pb/(Mg+Nb+Ti) ratio of 1.00 and an Mg/(Mg+Nb) ratio of 0.33.

The crystal structure and the orientation of the films were analyzed by x-ray diffraction (XRD) using a four-axis diffractometer (PANalytical X'Pert MRD). High-resolution XRD reciprocal space mapping[15] (HRXRD-RSM) was employed to analyze the crystal structure, including the film orientation, in- and out-of-plane lattice parameters, and the interaxial angle in detail. The composition of the film was measured with an x-ray fluorescence (XRF) spectrometer (PANalytical PW-2404), which was calibrated using sol-gel-derived standard samples and cross-checked by Rutherford backscattering spectrometry (RBS).

The electrical properties of the films were measured using $Pt/PMN-PT/SrRuO_3$ capacitors by fabricating 100-μm-diameter Pt top electrodes using an electron-beam evaporation method. The dielectric properties were measured at room temperature with an HP4194A impedance analyzer and the ferroelectric with a ferroelectric tester (Toyo Corp. FCE). Electric-field-induced displacement and the ferroelectric properties were simultaneously measured through a scanning probe microscope (SPM) (SII NanoTechnology Inc. SPI3800N) connected to a ferroelectric tester. A conductive cantilever was touched on the Pt top electrode using a contact mode. We used commercially available conductive diamond tips. The typical force constant of these tips was ~40 N/m for electrical conduction. Contact force was controlled at around several hundreds nanonewtons at all measurement points. Unipolar and bipolar driven voltages were applied to the samples with a drive frequency of 5 Hz, and the longitudinal displacement was evaluated using the proportional-integral-derivative-(PID) controlled Z-feedback signal of the SPM cantilever.[16] The effective longitudinal piezoelectric coefficient ($d_{33,f}$) was also measured with the SPM and a lock-in amplifier (NF Corporation LI5640),[17,18] which was calibrated using both x-cut quartz and a force curve. The oscillation frequency was set at 10 kHz and an ac voltage of 1 V (root mean square) was applied to induce surface vibration.

We fabricated the unimorph cantilever with dimensions of 6×1.5 mm^2 to measure the effective transverse piezoelectric coefficient ($e_{31,f}$) of the films. A 150-nm-thick Pt top electrode was deposited by sputtering before cutting the samples. Piezoelectric vibration was generated by means of applying sine wave voltage, and the tip displacement was measured using a laser Doppler velocity meter, after which $e_{31,f}$ was calculated.[19]

III. RESULTS AND DISCUSSION

A. Crystal structure

Figure 1 shows the change in XRD θ-2θ patterns with x for the films grown on $(100)_c SrRuO_3 \| (100)SrTiO_3$ substrates. (100)-/(001)-oriented films with no second phases, such as pyrochlore, were observed to have grown on these substrates irrespective of x. The epitaxial growth of all these films was also confirmed by x-ray pole figure measurements:

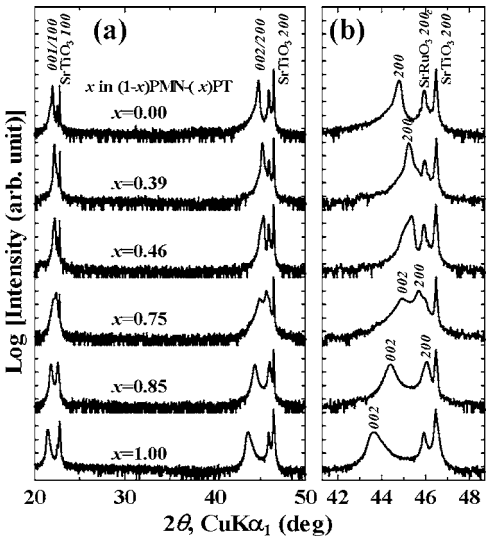

FIG. 1. XRD θ-2θ patterns for PMN-PT films with different PT content (x) grown on $(100)_c SrRuO_3 \| (100) SrTiO_3$ substrates in 2θ range (a) from 20° to 50° and (b) enlargement from 42° to 48°.

$(100)/(001)$PMN-PT$\|(100)_c SrRuO_3\|(100)SrTiO_3$. Figure 1(b) shows an enlarged one in the 2θ range from 42° to 48° shown in Fig. 1(a). PMN-PT 200 was observed for films with $x=0$ and 0.39. Both PMN-PT 002 and PMN-PT 200, on the other hand, were observed for films with $x=0.75$, 0.85, and 1. Note that the PMN-PT 200 peaks for the films with $x=0.85$ and 1 overlapped with the respective peaks for $SrRuO_3$ 200_c and $SrTiO_3$ 200. Finally, with $x=0.46$, an asymmetric peak was detected, even though it was very difficult to determine the detailed crystal symmetry for the PMN-PT phase from the θ-2θ scan. Therefore, HRXRD-RSM analysis was employed and Fig. 2 shows the change in the HRXRD-RSM results with x measured at around 204 $SrTiO_3$. The spot originated to rhombohedral (pseudocubic) PMN 204 was observed at $x=0$, as we can see from Fig. 2(a), while those originated to tetragonal PMN-PT 204 (one spot) and tetragonal PMN-PT 402 (three spots) were observed at $x=0.85$, as can be seen from Fig. 2(c). The lattice parameters and interaxial angle of these films were $a=b=c=4.045$ Å and 89.9° for the film with $x=0$, while they were $a=b=3.933$ Å, and $c=4.081$ Å and 90.0° for the film with $x=0.85$. A relatively large spot was observed for the film with $x=0.46$ as Fig. 2(b) shows. We tried to fit this spot into five spots for a mixed tetragonal and rhombohedral (pseudocubic) phases made up of four tetragonal spots and one rhombohedral spot by simulation fitting. This relatively large spot consisted of one spot of tetragonal PMN-PT 204, three spots of tetragonal PMN-PT 402, and one spot of rhombohedral (pseudocubic) symmetry, as can be seen from Fig. 2(b). Here, the lattice parameters and interaxial angle were $a=3.988$ and $c=4.024$ Å and $\beta=90.0°$ for the tetragonal symmetry and $a=3.999$ Å and $\alpha=89.9°$ for the rhombohedral (pseudocubic) symmetry. It is, however, very difficult to determine a detailed crystal symmetry by means of a conventional XRD system due to its relatively low accuracy compared with measurement with synchrotron radiation, as has been done by Noheda *et al.*[20] We also employed Raman spectroscopy to cross-check crystal symmetry, because it is

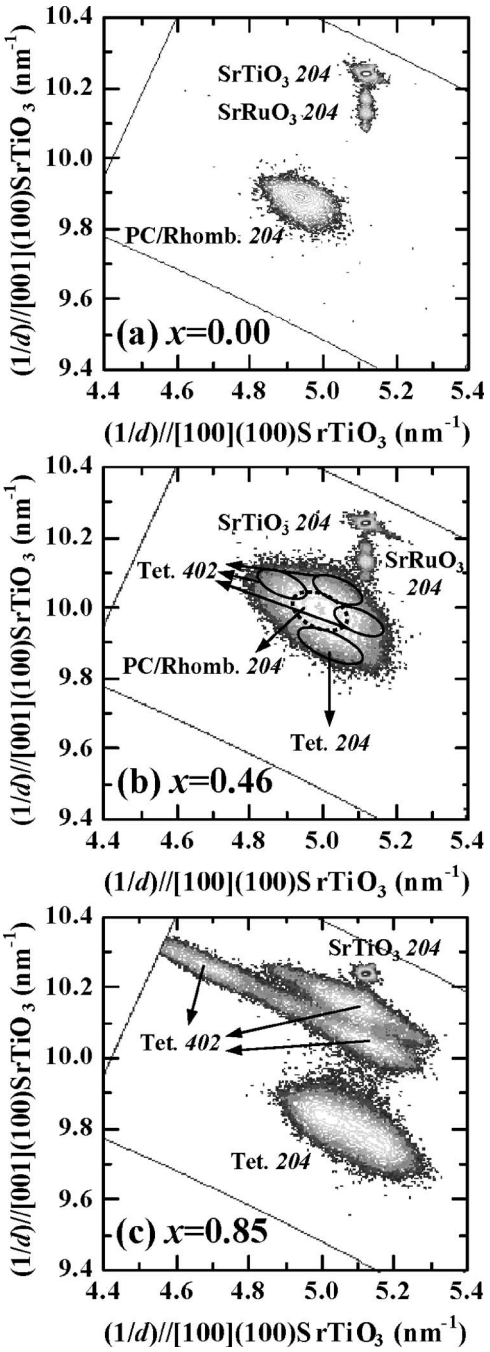

FIG. 2. High-resolution x-ray diffraction reciprocal space mappings (HRXRD-RSM) around $SrTiO_3$ 204 for PMN-PT film with x of (a) 0, (b) 0.46, and (c) 0.85. (Tet.: tetragonal and PC/Rhomb.: pseudocubic or rhombohedral).

very sensitive to this and the orientation. Figure 3 plots the Raman spectra at room temperature for epitaxial PMN-PT films with $x=0$, 0.42, and 0.85. The films with $x=0$ and 0.85 have typical spectra of cubic ($Fm\bar{3}m$) and tetragonal symmetries, respectively, and the shapes of the peaks are in good agreement with the data reported for sintered bodies and single crystals.[21–23] The Raman peak of the film with $x=0.42$, on the other hand, shows mixed spectra of cubic and tetragonal symmetries. This composition corresponds to the mixed phase of pseudocubic (rhombohedral) and tetragonal symmetries from the HRXRD-RSM results. As a result, the

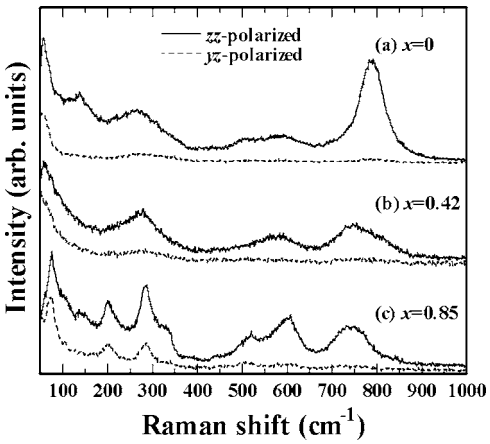

FIG. 3. The Raman spectra for PMN-PT films with different PT contents (x) grown on $(100)_c SrRuO_3 \| (100) SrTiO_3$ substrates. (a) $x=0$, (b) $x=0.42$, and (c) $x=085$. Respective solid lines and dashed lines show zz and yz scattering geometries that were adopted.

crystal symmetry of the films with $x=0.42$ was determined to be almost the same from both the Raman spectra and HRXRD-RSM.

Figure 4 shows the lattice parameters and the unit cell volume estimated from HRXRD-RSM analysis as a function of x. The reported lattice parameters and the constituent phases for PMN-PT single crystals[20] and the sintered body[24] are also shown in Fig. 4. The lattice parameters of PMN ($x=0$) and PT ($x=1$) films almost agreed with the reported data; however, there are relatively large deviations for PMN-PT, especially for the x ranging from 0.3 to 0.8, which is different to that for epitaxial PZT films grown on the same substrates,[25] in which the lattice parameters of the films almost agreed with the ones reported for bulk materials. This suggests that there is a large amount of residual strain in PMN-PT films. As we can see from Fig. 4, the mixture phase of rhombohedral (pseudocubic) and tetragonal symmetries was achieved at x values of around 0.40–0.55, which were higher than those reported for single crystals ($x=0.31-0.35$).[20] Such a large shift was not observed for epitaxial PZT films grown on the same $(100)_c SrRuO_3 \| (100) SrTiO_3$ substrates as we have already reported.[26] This difference between PZT and PMN-PT films is possibly due to the difference in growth conditions and/or materials parameters such as the difference between the deposition temperature and Curie temperatures, the thermal expansion coefficients, Young's moduli, and elastic compliance. Nagarajan *et al.*[27] pointed out that residual strain in epitaxial PMN-PT films influences the piezoelectric response and relaxor characteristics. These strains have an effect on the lattice parameters of the films and as a result possibly change their mixed phase region.

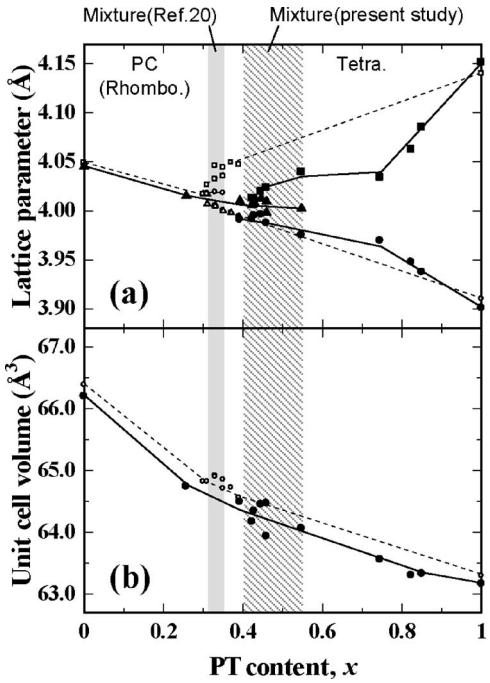

FIG. 4. Dependence of (a) lattice parameters and (b) unit cell volume of PMN-PT films on x value calculated from HRXRD-RSM results as closed symbols and solid lines. Reference data for single crystal (Ref. 20) and sintered body (Ref. 24) are also shown as open symbols and dotted lines, respectively. Constituent phases are also shown.

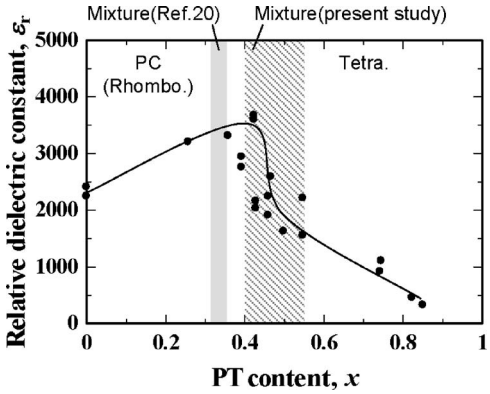

FIG. 5. Dependence of room temperature relative dielectric constant ε_r measured at 1 kHz on x value for (100)-/(001)-oriented epitaxial PMN-PT films. Constituent phases are also shown.

B. Electrical properties

Figure 5 shows room temperature relative dielectric constant ε_r measured at 1 kHz as a function of x, together with the constituent phase of the films estimated from the HRXRD-RSM results. ε_r was maximum at around $x=0.40$, corresponding to the film with the mixed phase. In addition, ε_r was larger in the rhombohedral (pseudocubic) films than in the tetragonal. This tendency was similar to that reported for a PMN-PT sintered body,[28] but its absolute value at room temperature was lower than those reported for a sintered body[28] and single crystals.[29] One possible reason is the shift of temperature showing the maximum ε_r, T_m, in the films compared with single crystals. In fact, T_m at 1 kHz was approximately 210 K for the 2.0-μm-thick epitaxial PMN ($x=0$) film, which was much lower than that for a sintered body, i.e., 263 K. Moreover, T_m at 1 kHz was approximately 400 K for the 2.8-μm-thick epitaxial PMN-PT ($x=0.39$) film. The T_m value of 400 K is reported for the single crystals[20] having x of 0.32. It must be mentioned that the T_m value of 400 K corresponds to the larger x edge of the rhombohedral phase region for both of film form ($x=0.39$, see Fig. 5) and single crystal ($x=0.32$), even though the correspond-

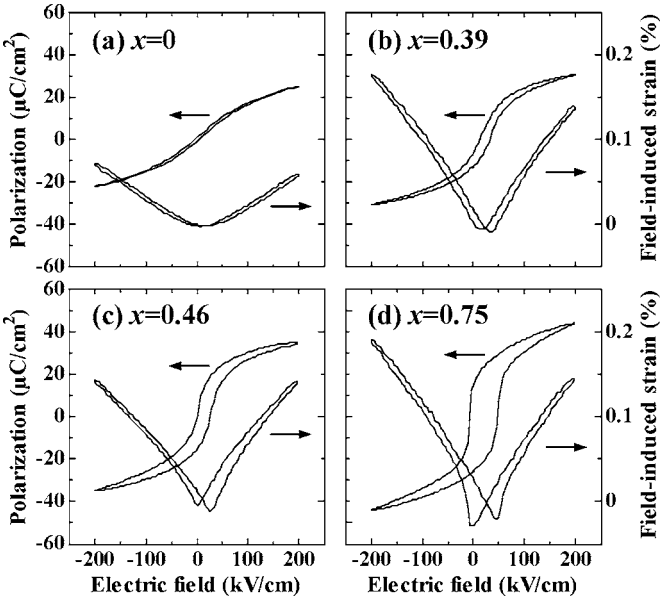

FIG. 6. Polarization and field-induced strain vs bipolar driven electric field simultaneously measured at 5 Hz for (100)-/(001)-oriented epitaxial PMN-PT films with x of (a) 0, (b) 0.39, (c) 0.46, and (d) 0.75.

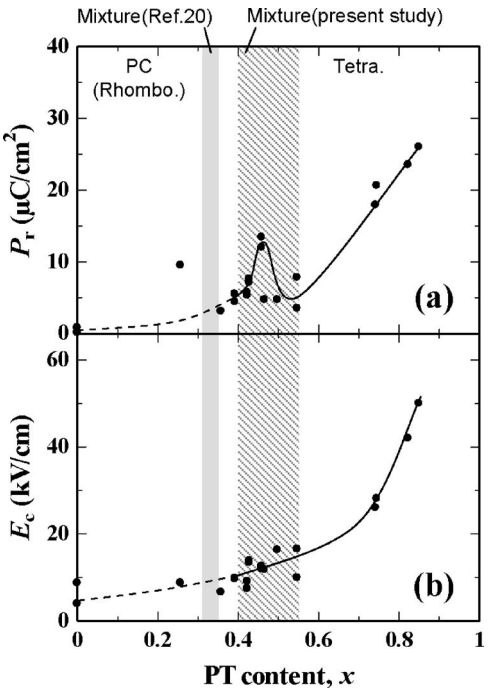

FIG. 7. Dependence of (a) remanent polarization P_r and (b) coercive field E_c measured at 5 Hz on x value for (100)-/(001)-oriented epitaxial PMN-PT films. Constituent phases are also shown. P_r and E_c values were obtained from the average of polarization (P) and electric field (E) across $E=0$ and $P=0$, respectively.

ing x values of film and the single crystal are not the same. The detailed investigation is under investigated.

Figure 6 shows the polarization versus electric field (P-E) and field-induced strain versus electric field (S-E) properties simultaneously measured at 5 Hz under electric fields applied up to 200 kV/cm for epitaxial PMN-PT films with x values of 0, 0.39, 0.46, and 0.75. Note that there are some imprints of hysteresis loops for all the films and the P-E hysteresis loops of the films with $x=0.46$ shown in Fig. 6(c) include the imprint data during the waiting time for applied time for starting hysteresis measurement after the polarization pulse. The remanent polarization P_r and the coercive field E_c of the films measured at 5 Hz as a function of the x value are summarized in Figs. 7(a) and 7(b). Averages of the polarization and electric field across electric field ($E=0$) and polarization axis ($P=0$) at plus and minus in Fig. 6 are, respectively, plotted as P_r and E_c in Fig. 7 to cancel the effect of imprint. P-E hysteresis loops for films with an x above 0.80 could not be measured due to their large leakage current. The P_r value had a peak at around $x=0.4$, which corresponds to the mixed phase region (near MPB composition), and increased above 0.55 (tetragonal region). In tetragonal PMN-PT films above $x=0.55$, the c/a ratio increased with increasing x, as shown in Fig. 4(a), which produced the larger c/a ratio. A large c/a ratio is considered to induce larger spontaneous polarization and the resulting P_r value is considered to increase with increasing x. We need to mention that the volume fraction of (001) orientation, i.e., polar axis orientation in mixed orientations of (001)/(100), was almost independent of x in the tetragonal single phase region. As can be seen from Fig. 7(b), the E_c value of the films monotonically increased with increasing x.

The absolute values of P_r for films with a mixed phase are relatively small and those for E_c are, respectively, large compared with the reported value for a (100) preferentially oriented sintered body having a similar composition.[30] Large E_c values are a common feature of films. Based on the fact that the P_r value showed relatively large film thickness dependency, the low P_r value of film is also possibly due to the thickness of the film.[31] Detailed film thickness dependency of the ferroelectricity is under investigated together with the temperature dependency for the films with different film thicknesses. Note that we have already reported that the P_r value did not strongly depend on crystal orientation.[32]

As can be seen in Fig. 6, slim loops, including field-induced polarization reported for PMN ceramics[33] were observed at $x=0$, while hysteresis originating to ferroelectricity was observed at $x=0.39$, 0.46, and 0.75. In addition, hysteresis of field-induced strain originating from typical ferroelectrics was observed at $x=0.39$, 0.46, and 0.75, as shown in Figs. 6(c) and 6(d), while this hysteresis was not observed at $x=0$. This indicates that the strain at $x=0$ was caused by the electrostrictive effect in which the field-induced strain was proportional to the square of the electric field (E^2). However, the strain above $x=0.39$ had good linearity at electric fields applied up to 200 kV/cm. It is very important to achieve the piezoelectric response that devices require. Note that the shapes of the P-E and S-E curves in Fig. 6 are similar to those of single crystals under uniaxial stress.[34] The P-E shape for the film with $x=0.39$ under residual strain, which was roughly calculated from the estimated lattice parameters from HRXRD-RSM results and the reference value,[20] is very similar to that of single crystal having the same rhombohedral symmetry under the same order of uniaxial stress. These results suggest that residual strain contributed not only to the crystal structure in Fig. 4 but also to both the ferroelectric and piezoelectric properties.

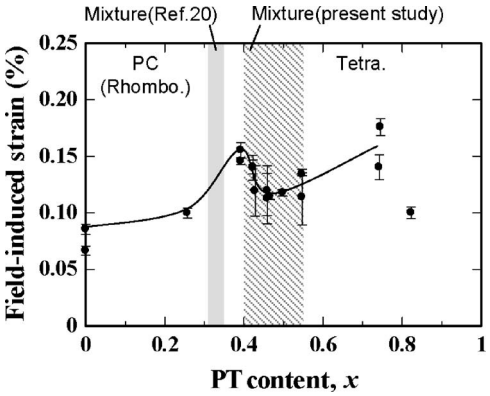

FIG. 8. Dependence of field-induced strain measured at applied electric field from 0 to 200 kV/cm and 5 Hz on x value for (100)-/(001)-oriented epitaxial PMN-PT films. Constituent phases are also shown.

The dependence the field-induced strain of the films had on x is summarized in Fig. 8. This value was calculated from unipolar driven S-E curves under electric fields applied from 0 to 200 kV/cm to the positive side and 5 Hz for parallel to the preferred polarization direction without long time poling Maria *et al.*[35] carried out. It was maximum at the larger x edge in the rhombohedral (pseudocubic) region. We also measured the $d_{33,f}$ and $e_{33,f}$ coefficients of these films and plotted them as a function of x in Figs. 9(a) and 9(b). The $d_{33,f}$ measured using a small ac voltage was in good agreement with that calculated using the S-E measurement slope shown in Fig. 6 and had a maximum value of 100–120 pm/V at the larger x edge in the rhombohedral (pseudocubic) phase region, $x=0.39$. The $e_{31,f}$ coefficient was also maximum at the same composition as that for $d_{33,f}$, as shown in Fig. 9(b), and was around -11.0 C/m^2. This

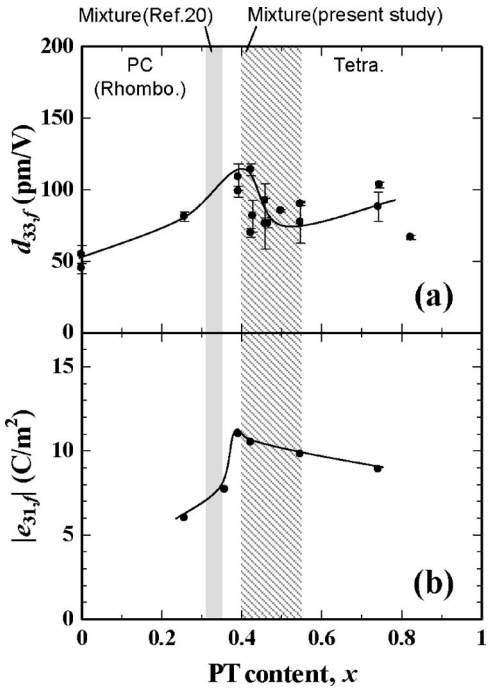

FIG. 9. Dependence of (a) longitudinal piezoelectric coefficient $d_{33,f}$ and (b) transverse piezoelectric coefficient $e_{31,f}$ on x value for (100)-/(001)-oriented epitaxial PMN-PT films. Constituent phases are also shown.

value was almost the same as the data reported for epitaxial PMN-PT film with $x=0.30$ prepared by pulsed laser deposition.[35] Both the in- and out-of-plane piezoelectric responses of epitaxial PMN-PT films had a maximum at the larger x edge in the rhombohedral (pseudocubic) phase region. This suggests that there is a relationship between the crystal structure and piezoelectric response in films, the same as for single crystals, despite the x value of 0.39, which is different from that required to obtain maximum piezoelectric response for single crystals.[2,3]

The transverse piezoelectric response in Fig. 9(b) has a higher value than that expected from longitudinal piezoelectric response. One reason is because of the effect of substrate clamping suggested by Lefki and Dormans[36] and Dubois *et al.*[37] The stress state in films is quite different from that in single crystals, i.e., extra two-dimensional stress from the substrate is applied to films, which is not applied to a three-dimensional-free sintered body and single crystals, and this places restrictions on electrically induced displacement especially on in-plane directions. This stress possibly affects the electromechanical response and the crystal structure of the films as previously mentioned.[34]

Orientation of the film is another important factor because the [001] orientation of PMN-PT is suggested to show the special domain alignment as Shrout *et al.*[2] and Park and Shrout[3] pointed out. The systematic investigation of the transverse and the longitudinal piezoelectric response research is under investigated using (100)-, (110)-, and (111)-oriented epitaxial PMN-PT films with different x values.

IV. CONCLUSIONS

The effects x had on the crystal structure, dielectric, ferroelectric, and piezoelectric properties of (100)-/(001)-oriented epitaxial PMN-PT films, 2–3 μm in thickness, grown on $(100)_c SrRuO_3 \| (100) SrTiO_3$ substrates at 650 °C by MOCVD were systematically investigated in view of the residual strain in the film. HRXRD-RSM results showed that the constituent phase of the films changed from a rhombohedral (pseudocubic) single phase, a mixture phase of rhombohedral (pseudocubic) and tetragonal phases, and a tetragonal single phase with an increase in x. The mixed phase region was observed at around x values of 0.40–0.55, which was larger than those reported for sintered bodies and single crystals (around x values of 0.31–0.35). The dependencies of ε_r and P_r on x showed similar tendencies for sintered bodies. However, their magnitudes were lower than those for bulks. The longitudinal field-induced strain and $d_{33,f}$ were also lower than the reported values for sintered body and single crystals. These lower longitudinal piezoelectric responses of the films, together with their lower ε_r and P_r values, suggest that the existence of residual strain contributed to these properties. The $e_{31,f}$ coefficient, on the other hand, may possibly have been enhanced for films by in-plane stress from the substrate. Despite the fact that the mixed phase region in films appeared at a higher x value than the case of single crystals which corresponded to the large amount of residual strain, the piezoelectric response was in good agreement with the constituent phase. As a result, both in- and out-of-plane

piezoelectric coefficients were maximum at the higher x edge in the rhombohedral (pseudocubic) phase region conforming to the engineered domain concept that is widely accepted for relaxor-type ferroelectric single crystals.

ACKNOWLEDGMENTS

The authors are thankful to Professor Seiichiro Koda and Professor Hiroshi Uchida of Sophia University for helping with the XRF analysis, and to Professor Alexei Gruvermann of North Carolina State University and Professor Masaru Shimizu and Professor Fujisawa of the University of Hyogo for helping with the SPM measurements.

[1]L. E. Cross, Ferroelectrics **151**, 305 (1994).
[2]T. R. Shrout, Z. P. Chang, N. Kim, and S. Markgraf, Ferroelectr., Lett. Sect. **12**, 63 (1990).
[3]S. E. Park and T. R. Shrout, IEEE Trans. Ultrason. Ferroelectr. Freq. Control **44**, 140 (1997).
[4]S. Trolier-McKinstry, J. F. Shepard, J. L. Lacey, T. Su, G. Zavala, and J. Fender, Ferroelectrics **206–207**, 381 (1998).
[5]J. P. Maria, W. Hackenberger, and S. Trolier-McKinstry, J. Appl. Phys. **84**, 5147 (1998).
[6]J. H. Park, F. Xu, and S. Trolier-McKinstry, J. Appl. Phys. **89**, 568 (2001).
[7]S. D. Bu, M. K. Lee, C. B. Eom, W. Tian, X. Q. Pan, S. K. Streiffer, and J. J. Krajewski, Appl. Phys. Lett. **79**, 3482 (2001).
[8]A. Laha, S. Saha, and S. B. Krupanidhi, Thin Solid Films **424**, 274 (2003).
[9]Y. Takeshima, K. Shiratsuyu, H. Takagi, and K. Tomono, Jpn. J. Appl. Phys., Part 1 **34**, 5083 (1995).
[10]S. Stemmer, G. R. Bai, N. D. Browning, and S. K. Streiffer, J. Appl. Phys. **87**, 3526 (2000).
[11]Y. Honda, S. Yokoyama, and H. Funakubo, Trans. Mater. Res. Soc. Jpn. **28**, 157 (2003).
[12]S. Yokoyama *et al.*, J. Appl. Phys. **98**, 086112 (2005).
[13]K. Nagashima, M. Aratani, and H. Funakubo, Jpn. J. Appl. Phys., Part 2 **39**, L996 (2000).
[14]A. Sumi, K. Takahashi, S. Yokoyama, H. Morioka, M. Yoshimoto, and H. Funakubo, Appl. Phys. Lett. **87**, 052112 (2005).
[15]K. Saito, T. Kurosawa, T. Akai, T. Oikawa, and H. Funakubo, J. Appl. Phys. **93**, 545 (2003).
[16]H. Maiwa and N. Ichinose, Jpn. J. Appl. Phys., Part 1 **39**, 5403 (2000).
[17]C. Harnagea, A. Pignolet, M. Alexe, D. Hesse, and U. Gösele, Appl. Phys. A: Mater. Sci. Process. **70**, 261 (2000).
[18]S. V. Kalinin, E. Karapetian, and M. Kachanov, Phys. Rev. B **70**, 184101 (2004).
[19]J. G. Smits and W. S. Choi, IEEE Trans. Ultrason. Ferroelectr. Freq. Control **38**, 256 (1991).
[20]B. Noheda, D. E. Cox, and G. Shirane, Phys. Rev. B **66**, 054104 (2002).
[21]G. Burns and B. A. Scott, Phys. Rev. Lett. **25**, 1191 (1970).
[22]H. Idink and W. B. White, J. Appl. Phys. **76**, 1789 (1994).
[23]H. Ohwa, M. Iwata, H. Orihara, N. Yasuda, and Y. Ishibashi, J. Phys. Soc. Jpn. **70**, 3149 (2001).
[24]*Ferroelectrics and Related substances*, Landolt-Bornstein, New Series, Group III, Vol. III/36A (Springer-Verlag, Berlin-Heidelberg-New York, 2001-2002).
[25]S. Yokoyama, Y. Honda, H. Morioka, S. Okamoto, T. Iijima, H. Matsuda, K. Saito, and H. Funakubo, Integr. Ferroelectr. **64**, 217 (2004).
[26]S. Yokoyama *et al.*, J. Appl. Phys. **98**, 094106 (2005).
[27]V. Nagarajan, S. P. Alpay, C. S. Ganpule, B. K. Nagaraj, S. Aggarwal, E. D. Williams, A. L. Roytburd, and R. Ramesh, Appl. Phys. Lett. **77**, 438 (2000).
[28]S. W. Choi, T. R. Shrout, S. J. Jang, and A. S. Bhalla, Ferroelectrics **100**, 29 (1989).
[29]R. Zhang, B. Jiang, and W. Cao, J. Appl. Phys. **90**, 3471 (2001).
[30]E. M. Sabolsky, A. R. James, S. Kwon, S. Trolier-McKinstry, and G. L. Messing, Appl. Phys. Lett. **78**, 2551 (2001).
[31]J. S. Speck and W. Pompe, J. Appl. Phys. **76**, 466 (1994).
[32]S. Yokoyama, S. Okamoto, S. Okamoto, T. Iijima, K. Saito, H. Okino, T. Yamamoto, and H. Funakubo, Integr. Ferroelectr. **80**, 67 (2006).
[33]J-F. Li and D. Viehland, J. Appl. Phys. **80**, 3451 (1996).
[34]Z. Feng, D. Li, H. Luo, S. Li, and D. Fang, J. Appl. Phys. **97**, 024103 (2005).
[35]J. P. Maria, J. F. Shepard, Jr., S. Trolier-McKinstry, T. R. Watkins, and A. E. Payzant, Int. J. Appl. Ceram. Technol. **2**, 51 (2005).
[36]K. Lefki and G. J. M. Dormans, J. Appl. Phys. **76**, 1764 (1994).
[37]M. A. Dubois, P. Muralt, D. V. Taylor, and S. Hiboux, Integr. Ferroelectr. **22**, 535 (1998).